Progress in Natural Science: Materials International 31 (2021) 865–871

HOSTED BY

Contents lists available at ScienceDirect

Progress in Natural Science: Materials International

journal homepage: www.elsevier.com/locate/pnsmi

Original Research

Nanomembrane folding origami: Geometry control and micro-machine applications

Yang Zong [a,b,1], Xinyuan Zhang [a,b,1], Yue Wu [a,b], Yang Wang [a,b], Chang Liu [a,b], Borui Xu [a,c,d], Gaoshan Huang [a,b,d], Jizhai Cui [a,b,d,*], Yongfeng Mei [a,b,c,d,*]

[a] Department of Materials Science, State Key Laboratory of ASIC and Systems, Fudan University, 220 Handan Road, Shanghai, 200433, China
[b] International Institute for Intelligent Nanorobots and Nanosystems, Fudan University, 2005 Songhu Road, Shanghai, 200438, China
[c] Shanghai Frontiers Science Research Base of Intelligent Optoelectronics and Perception, Institute of Optoelectronics, Fudan University, 220 Handan Road, Shanghai, 200433, China
[d] Yiwu Research Institute of Fudan University, Chengbei Road, Yiwu City, 322000, Zhejiang, China

ARTICLE INFO

Keywords:
Folding origami
Liquid-triggered delamination
Strain engineering
Magnetic manipulation
Micro-machine

ABSTRACT

Three-dimensional (3D) microstructures have important applications in a wide range of engineering fields. A strategy of nanomembrane folding origami with microdroplet-guided intercalation and strain engineering to construct complex 3D microstructures for micro-machine applications is proposed in the present investigation. The results showed that nanomembranes were released by the microdroplet intercalation and subsequently fold up as creases, or remain flat as facets, depending on the strain design configurations. The 3D geometry can be controlled by the crease design and by an externally applied magnetic field. Moreover, this folding strategy is used to construct magnetic micro-mirror arrays, magnetic micro-robots, and a twin-jet motor platform, showing potential micro-machine applications in optical micro-devices and robotics. This strategy offers a simple, precise, and designable method of folding 3D microstructures for fundamental research and practical applications.

1. Introduction

Three-dimensional (3D) microstructures received wide interest in the past decades due to their great promise in micro/nano-electromechanical systems (MEMS/NEMS) [1–3], robotics [4–8], biomimetic systems [9], and mechanical metamaterials [10–12]. While significant progress has been made for the fabrication of planar devices, directly fabricating complex 3D microstructures remains very challenging [13]. Alternatively, the concept of origami, which is the art of folds planer sheets into sophisticated 3D structures, has been introduced to the fabrication of 3D microstructures, taking advantage of the well-developed planar fabrication techniques [14–17].

Fabrication of the 3D microstructure using the origami concept, requires releasing the originally flat nanomembranes from the substrate, and then folding or rolling them towards the third dimension. Generally, nanomembranes can be released by wet etching [18–22] or dry etching [23,24] of sacrificially layers underneath. These are parallel fabrication methods and therefore are suitable for mass fabrication. Recently, a general strategy of releasing individual nanomembrane devices on-demand is reported [25]. By positioninga micro-droplet on the edge of a target device, the droplet intercalates in between the nanomembrane and the substrate, triggering deterministic rolling of the nanomembrane in various configurations. However, this strategy allows only rolling origami, in which the whole device rolls up altogether, limiting its application to 3D tubular microstructures. Complex micro-origami structures, such as polyhedron and Miura-ori structures [26,27], require that only designed regions fold or roll up as folding creases, while other regions remain flat as facets.

In this work, we developed a strategy of folding origami based on strain engineering and microdroplet-guided delamination of nanomembranes. The creases and facets are achieved by engineering the strain configuration of local regions. A pre-layer, composed of

* Corresponding authors.
E-mail addresses: jzcui@fudan.edu.cn (J. Cui), yfm@fudan.edu.cn (Y. Mei).
[1] These authors contributed equally.

https://doi.org/10.1016/j.pnsc.2021.09.010
Received 15 August 2021; Received in revised form 14 September 2021; Accepted 23 September 2021
Available online 13 December 2021

sequentially deposited nanomembranes with a designed strain gradient, is firstly deposited. A second layer, composed of deposited nanomembranes in reversed order (therefore with opposite strain gradient), is deposited to offset the strain from the pre-layer. When the microstructure is released, the regions with only the pre-layer roll up because of its strain gradient, serving as creases; the regions with both the pre-layer and the second layer remain flat since the strain of both layers is counterbalanced, serving as facets of the micro-origami. We achieve the geometry control of folding angle through the crease design and magnetic manipulation. The folding angle of the crease can be adjusted by tuning its length. By adding a magnetic layer, the folding angle can be adjusted by an externally applied magnetic field. Based on this concept, we demonstrate several origami-inspired micro-machines including an array of magnetic micro-mirrors, a magnetic micro-robot, and a twin-jet micromotor platform. Our strategy serves as an effective method for the fabrication of 3D microstructures with wide applications in micro-optics, micro-robotics, and metamaterials.

2. Experiment details

2.1. Microdroplet-guided delamination for 3D microstructure construction

A capillary containing ethanol was used to release microdroplets to guide the delamination of nanomembrane and substrate. The tip of the capillary containing ethanol was placed on the surface. Due to the capillary force and surface tension, the microdroplet was ejected between the substrate and capillary. The motion control of the microdroplet on the surface of the substrate was realized by controlling capillary through a micromanipulator, which triggered the separation between the nanomembrane and substrate.

2.2. Deposition of nanomembranes

The nanomembranes are deposited on a glass substrate by electron beam evaporation (TSV-700, Tenstar Vacuum). There were five kinds of nanomembranes used in this article: Fe (thickness: 40 nm; evaporation rate: 1.5 Å/s), Ti (thickness: 40 nm; evaporation rate: 1.5 Å/s), Ag (thickness: 40 nm; evaporation rate: 1.5 Å/s), TiO_2 (thickness: 100 nm; evaporation rate: 0.5 Å/s), and Pt (thickness: 2 nm; evaporation rate: 0.5 Å/s). By adjusting the deposition rate, the strain of each layer could be controlled. Stacking nanomembranes with different strains in sequence can generate a specific strain gradient. There were two types of stacked multilayer nanomembranes used in this study: Ag/Ti/Fe multilayer (strain gradient with tensile strain on the top and compressive strain on the bottom) and Fe/Ti/Ag multilayer (strain gradient with compressive strain on the top and tensile strain on the bottom). With the aid of different shadow masks, the patterned multilayer nanomembranes could be obtained.

2.3. Magnetic manipulation

NdFeB magnet and Helmholtz coil were used to apply a magnetic field. A NdFeB bar magnet was used to apply the magnetic field, along the its magnetization direction, to our folding structure. With the aid of linear precision stage, the distance between magnet and folding structure along the magnetization direction could be tuned, which can adjust the strength of magnetic field from 0 to 80 mT while keeping the same magnetic field direction [28]. The strength of magnetic field was measured by a magnetometer (TD8620, TUNKIA) during this process. In this work, the magnetic gradient force generated on the folding facets is extremely small, therefore the torque caused by magnetic gradient force is ignored. Helmholtz coil applies a rotating magnetic field (5 Hz, 10 mT) with the aid of the LabView program to manipulate the motion of magnetic micro-robot.

2.4. Device characterization

The morphologies of folding structures, magnetic micro-mirror arrays, magnetic micro-robot, and twin-jet micro-motor platforms were characterized by scanning electron microscopy (Sigma FESEM, ZEISS) and optical microscopy (SmartZoom5, ZEISS; BX51, OLYMPUS). The folding angles of folding structures were measured by their SEM or optical microscopy images. As for magnetic micro-mirror arrays, optical microscopy (SmartZoom5, ZEISS) was also used to apply the light source (light source on microscopy) and camera (CCD camera on microscopy). The manipulation of magnetic micro-robot was experimented in 1.5 wt% polyvinyl alcohol (PVA) aqueous solution with 0.48 wt% sodium dodecyl benzene sulfonate (SDBS). The self-driven motion of twin-jet micromotor was tested in 5% hydrogenperoxide solution. All the experimental videos were recorded by the CCD cameras attached to the corresponding optical microscopy.

3. Result

3.1. Construction of folding structures

Complex 3D folding microstructures were achieved by folding origami with microdroplet-guided intercalation and strain engineering, as shown in Fig. 1. The concept of liquid-triggered delamination is depicted in Fig. 1a. A strained nanomembrane as a pre-layer was deposited on the substrate to create a van der Waals interaction with the substrate. During the release process, a capillary was brought to be in contact with the substrate and released a micro-droplet. The micro-droplet flowed on the surface, and when it contacted the edge of nanomembranes, intercalated in between the substrate and the nanomembrane. The intercalation breaks the van der Waals contacted between the substrate and strained nanomembrane, which triggers the separation of nanomembrane and substrate. Because of the intrinsic strain gradient within the nanomembrane generated during the deposition process, the nanomembrane rolled up after being released from the substrate.

Based on the liquid-triggered delamination method, the strain gradient configuration within the nanomembranes to form 3D folding structures was engineered, which is presented in Fig. 1b and c. The multiple layers of nanomembrane were deposited on the substrate by electron beam evaporation system. By adjusting the evaporation rate and thickness of each layer, a strain gradient with tensile strain on the top and compressive strain on the bottom can be created in the nanomembranes, which is named “Type A″ shown in Fig. 1b. After being released by the liquid-triggered delamination the top surface shrunk to release the tensile strain and the bottom surface expended to release the compressive strain, resulting in the whole Type A nanomembrane stack bending upwards. By reversing the order of nanomembrane deposited the strain gradient and bending direction were reversed as well, which is named as “Type B″ shown Fig. 1b. Both types of strain gradients lead to the rolling of the whole nanomembrane as tubular 3D structures, as indicated by the scanning electron microscopy images shown in Fig. 1b.

Based on these two types of strain design, the flat facets and folding creases can be created. These two types of multilayer nanomembranes with opposite strain gradients can be stacked together to balance the strain, forming an undeformed flat plane (Fig. 1c). To be specific, when type A nanomembranes were deposited as a continuous pre-layer and type B nanomembranes were deposited on top of type A nanomembranes and patterned, the regions with both the Type A and Type B layers remained flat, and the regions with only the Type A layers bended up. These two different regions serve as the rigid facets and bendable creases in the origami design concept, respectively [29]. Thus, a folding structure with a bending crease and two flat facets could be constructed after the release process. The scanning electron microscope (SEM) images in Fig. 1b and c elucidate the bending and folding structure after the release process, which shows the successful transformation from bending to folding.

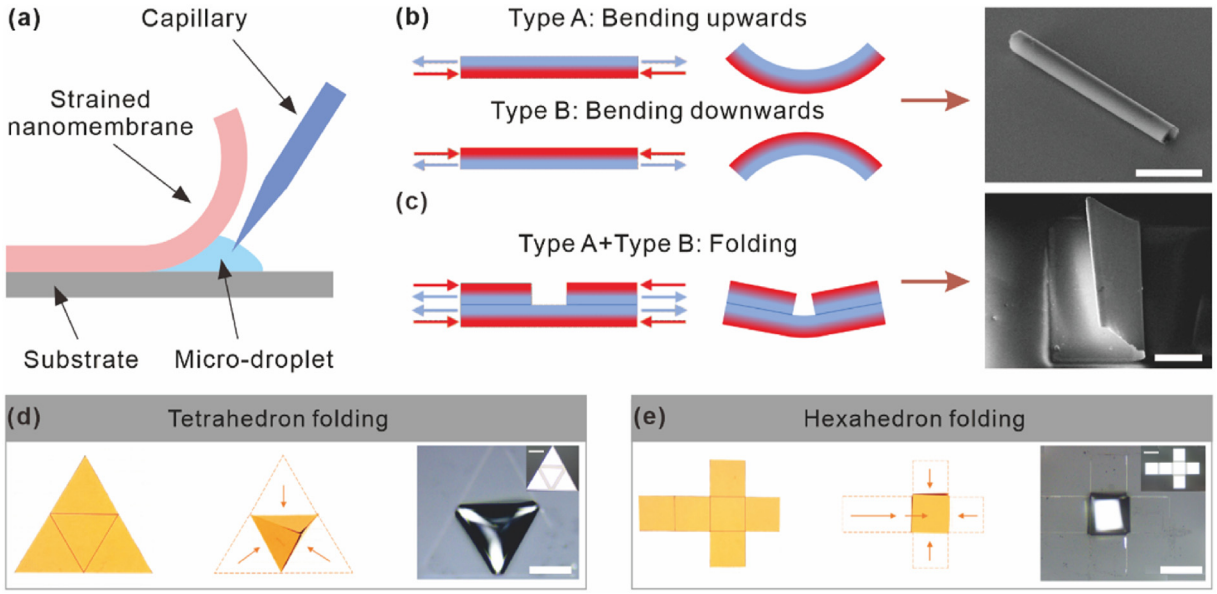

Fig. 1. Folding structure construction by microdroplet-guided intercalation and strain engineering. (a) Schematic illustration of the release process of nanomembrane by microdroplet. (b) Schemes of strain design of rolling structures with two types of strain gradient, and SEM image of the corresponding rolling microstructure. The red arrow represents compressive strain direction and the blue arrow represents tensile strain direction. Scale bar, 100 μm. (c) Schemes of strain design of folding microstructures and SEM image of the folding structure. Scale bar, 100 μm. (d) Tetrahedron and (e) Hexahedron paper origami before and after folding (left and middle images) and nanomembranes microstructure after and before folding (right images and the inset). Yellow arrows and dotted lines indicate the direction of folding and the outline before folding. Scale bars, 100 μm.

Benefiting from liquid-triggered delamination release process and strain design, this micro-scale nanomembrane with nanometer thickness could be folded up sequentially with designed creases like paper origami to create polyhedral folding, as shown in Fig. 1d and e. Two different patterned multilayer nanomembranes (Type A and Type B) were successively deposited on the glass substrate to create the folding pattern

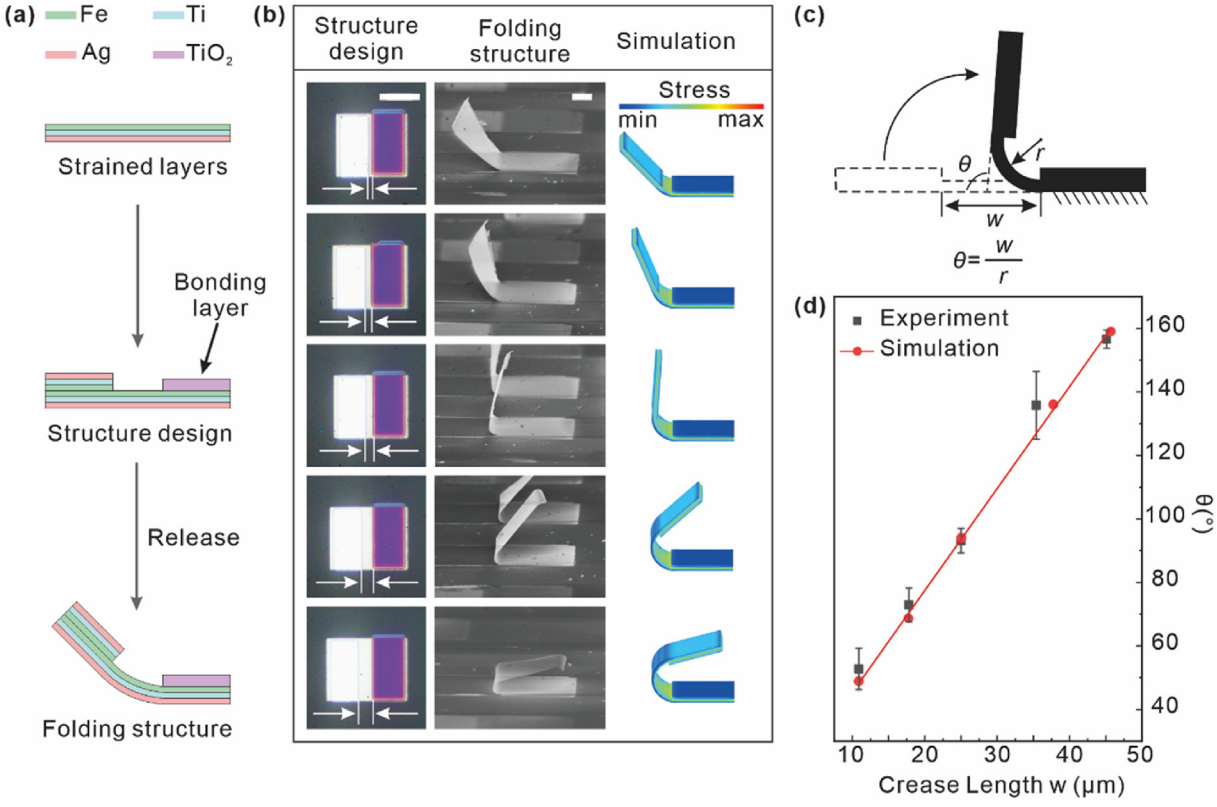

Fig. 2. Controlling folding angle by crease design. (a) Schematic of the fabrication process of a folding structure. (b) Controlling folding angle by adjusting crease length. The first column is the optical microscopy images of structures with different crease lengths before being released. Scale bar, 50 μm. The second column is the SEM images of folding structures with different folding angles. Scale bar, 30 μm. The third column is the results of the corresponding simulation results. (c) Schematic of crease design and corresponding folding angle. (d) Relationship between the folding angle θ related to the crease length w.

with creases and flat planes. Then the folding pattern was folded up sequentially from its peripheral to the center like paper origami. At last, tetrahedron and hexahedron three-dimensional microstructure could be obtained. Based on this strategy of folding origami with microdroplet-guided intercalation and strain engineering, a complex 3D folding microstructure was fabricated.

3.2. Controlling folding angle by crease design

Base on the construction of the folding structure above the crease design was investigated to precisely control the folding angle, which is presented in Fig. 2. A single folding structure (two facets with a single crease in between) was fabricated according to the process flow shown in Fig. 2a. Firstly, a shadow mask was used to pattern the strained layer. Ag/Ti/Fe multilayers with each layer 40 nm thickness were deposited in order by the electron beam evaporation system with the evaporation rate of 1.5/1.5/1.5 Å/s on the glass substrate to create van der Waals contact with the substrate. The other two rounds of electron beam evaporation along with corresponding shadow masks were performed, which define the folding facet (Fe/Ti/Ag, 40/40/40 nm, 1.5/1.5/1.5 Å/s evaporation rate) and the bonding layer (TiO_2, 100 nm, 0.5 Å/s evaporation rate), respectively. At last, a capillary was used to eject a micro-droplet to release the folding facet, after which the crease rolled up.

Based on the fabrication above, the folding angle can be precisely controlled by the crease length, w, which can be easily controlled by adjusting the size of shadow masks. Several structure designs with different crease lengths w were obtained, which is shown in the first column in Fig. 2b. When released by liquid-triggered delamination the microstructures with different crease lengths demonstrated different folding angles, as shown in SEM images in the second column of Fig. 2b. Furthermore, these structure designs are modeled in COMSOL Multiphysics according to the corresponding experimental parameters (materials and crease length). The internal strain of each layer was set, and a strain gradient was created. The TiO_2 bonding part layer was set as a fixed constraint with no deformation in the simulation, while the other sides were set free. With the aid of this finite element analysis the final structures of folded-up microstructures could be precisely predicted with assigned patterns and crease lengths. This phenomenon can be described by the model developed in Fig. 2c. The strain gradient within the nanomembranes determines the radius of curvature r of the crease. The folding angle θ can be calculated as $\theta=w/r$, where w is the length of the crease. According to this relation, for the nanomembranes with the same strain gradient (therefore having the same radius of curvature), increasing crease length leads to the linear increase of the folding angle, which is shown in Fig. 2d. In summary, the folding angle can be precisely controlled through the design of the crease. The linear relationship between the folding angle and the crease length can easily guide the design of the required folding angle.

3.3. Magnetic manipulation of the folding angle

The folding angle of the microstructure can be further manipulated after the release by applying an external magnetic field. The Fe layer is magnetized with a magnetic moment m in the facet plane when applied with a magnetic field B and therefore tends to align to the field direction actuated by a magnetic torque $\boldsymbol{\tau}=\boldsymbol{m}\times\boldsymbol{B}$ [30]. This magnetic torque can be used to adjust the folding angle of the microstructure. The experiments were performed to investigate the structure's folding angle under the magnetic field ranging from 0 to 80 mT upwards perpendicular to the substrate observed from the top view and side view (Fig. 3a). As the magnitude of the magnetic field increases, the folded plane gradually decreases its folding angle to deflects towards the direction of the magnetic field. A magneto-mechanical model is depicted in Fig. 3b. The folding angle reaches $\theta=\theta_0$ after the facet being released from the substrate without the external magnetic field. When a certain magnetic field intensity B is applied to the folded structure perpendicular to the substrate, the facet is magnetized with magnetic moment m within the facet plane. Then a magnetic torque can be generated:

$$\tau_{magnetic} = M_s abt_m B cos\theta \quad (1)$$

where $\tau_{magnetic}$ is magnetic torque, θ_m is the angle of deflection because of

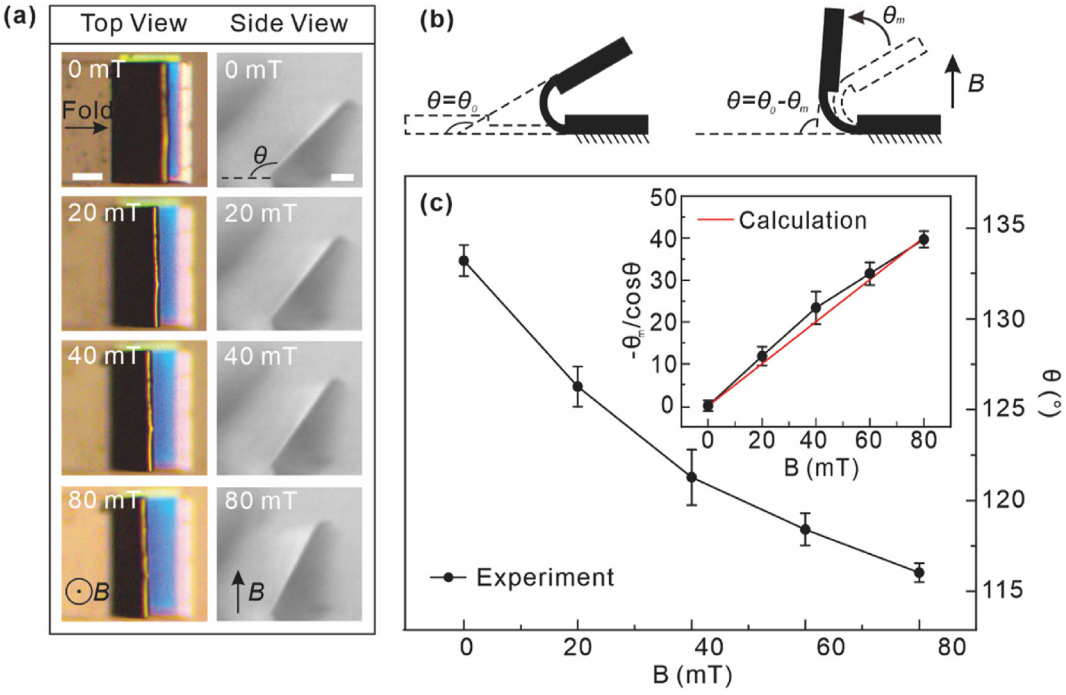

Fig. 3. Magnetic manipulation of the folding angle. (a) The top and side view optical microscope images of folding structures in different magnetic fields. Scale bars, 25 μm. (b) The schemes of angular deflection of the folding structure before and after an applied magnetic field. (c) Relationship between the applied magnetic field B and the folding angle θ. The inset is the relationship between the applied magnetic field B and $\frac{-\theta_m}{\cos\theta}$.

the magnetic field, θ is the total folding angle, M_s is the saturation magnetization of the magnetic layer Fe, a and b are the length and width of folding facet, t_m is the thickness of Fe magnetic layer, and B is the applied magnetic field. This torque leads to the change of the total folding angle θ from θ_0 to θ_0-θ_m, when applied with the magnetic field B. This angle deflection will produce an elastic deformation of the crease, which will cause an elastic torque opposite to the magnetic torque.

$$\tau_{elastic} = \frac{ct^3E}{12w}\theta_m \tag{2}$$

where w, c, t, E are the length, width, thickness, and Young's modulus of the crease. According to our design, c=b (in Equation (1)). When the magnetic-induced torque and elastic torque are balanced, i.e. $\tau_{magnetic}+\tau_{elastic}=0$, the relationship between the magnetic field B and the folding angle θ can be established:

$$-\frac{\theta_m}{\cos\theta} = \frac{12wM_sat_m}{Et^3}B \tag{3}$$

The experimental and calculation results of folding angle θ and magnetic field intensity B are plotted in Fig. 3c, which shows that the folding angle θ decreases with the increase of the magnetic field B. According to formula (3), $\frac{-\theta_m}{\cos\theta}$ and B are in a linear relation. The inset of Fig. 3c clearly shows that both the experiment and simulation closely follow the linear relation. The calculation results match the experimental results very well. In conclusion, magnetic fields can accurately tune the folding angle of the folding structures.

3.4. Functional micro-machines

The folding origami with microdroplet-guided intercalation and strain engineering has great potential in 3D functional micro-machines. Here, three different demonstrations of device application with this approach of the folding origami were presented. A magnetic micro-mirror array is established with this folding origami concept, as shown in Fig. 4a–i. Through the strain gradient design, the flat facet can be used as micro-mirrors and reflects light. The folding angle can be controlled with magnetic manipulation, therefore tuning the light reflection angles. When changing to a specific angle, the reflected light can be received by a camera in a fixed direction. At the same time, using the release process of microdroplet-guided intercalation, the mirror can be released at desired positions while the others kept unreleased, forming a designed array. The SEM in Fig. 4a–ii demonstrates an SEM image of a 2 × 2 array with two released micro-mirrors, and the other two unreleased. Based on this idea, we designed two patterned arrays of 'F' and 'D' which are shown in Fig. 4a–iii and Supplementary Video 1. The 'F' and 'D' micro-mirrors arrays are shown as bright and dark in the microscope controlled by magnetic manipulation. When the micro-mirrors are deflected to a certain angle by an applied magnetic field, the light reflects into the camera of the microscope, so that the micro-mirror regions are shown as bright, as shown in Fig. 4a–iii. When the micro-mirrors are away from this perfect deflection angle, controlled by the magnetic field, the light reflects away from the camera, so that the micro-mirrors regions are dark, as shown in Fig. 4a–iii. This device demonstrates the function of controlling lens reflection angle by a magnetic field, which shows that our folding origami design can be used to fabricate specifically arranged micro-mirror arrays.

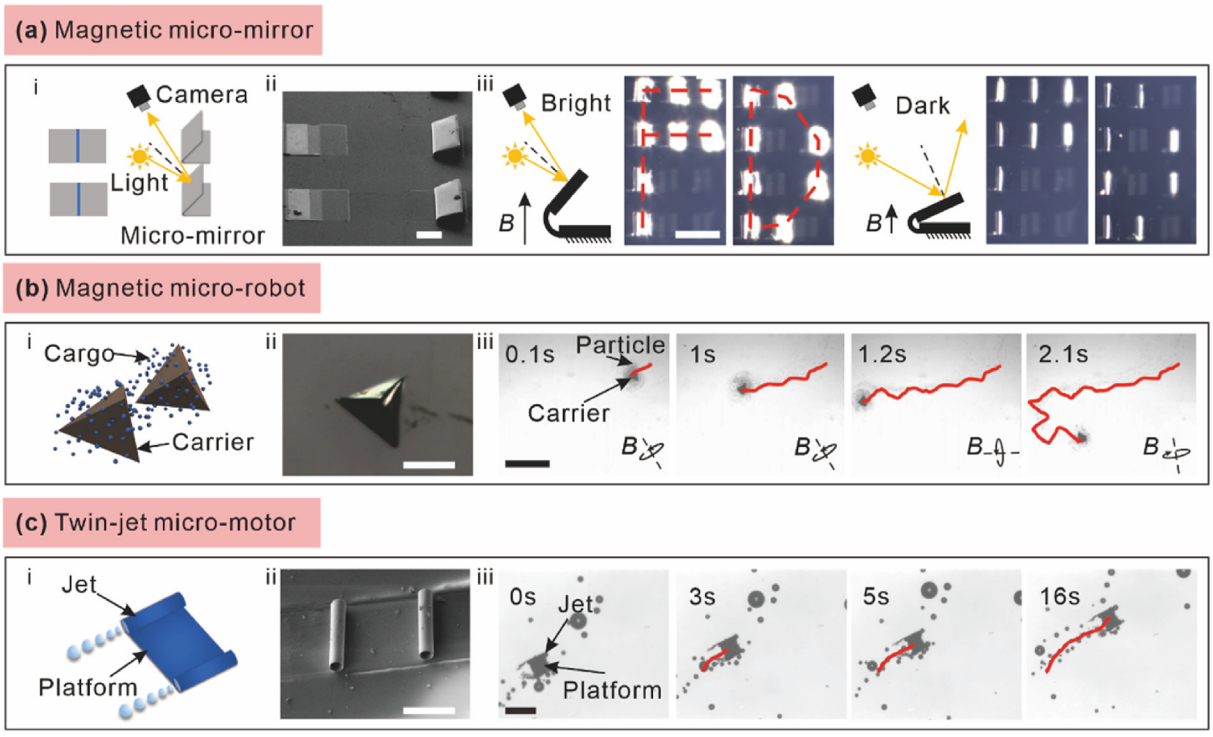

Fig. 4. Functional micro-machines based on folding origami microstructures. (a) Magnetic micro-mirrors based on an on-chip array of folding structures. i, reflection mechanism of micro-mirrors. ii, SEM image of a 2 × 2 array with two released micro-mirrors and the other two kept unreleased. Scale bar, 100 μm iii, the bright and dark states in the experiment by adjusting the magnetic field. Scale bar, 200 μm. (b) The magnetic tetrahedron micro-robot by folding origami. i, scheme of cargo transportation by magnetic tetrahedron micro-robot. ii, optical microscopy image of magnetic tetrahedron micro-robot. Scale bar, 200 μm iii, polystyrene beads with 5 μm diameter transportation by magnetic tetrahedron micro-robot by its surrounding flow field caused by the rotational motion under the applied rotating magnetic field. Scale bar, 600 μm. (c) Twin-jet micro-motor platform. i, scheme of twin-jet micro-motor platform composed of two tubular catalytic jets to generate driving force and a flat plane in middle. ii, the SEM image of the twin-jet micro-motor platform. Scale bar, 50 μm iii, the motion of twin-jet micro-motor platform in 5% hydrogen peroxide solution. Scale bar, 300 μm.

Supplementary video related to this article can be found at https://doi.org/10.1016/j.pnsc.2021.09.010

The second demonstration is based on the construction of a 3D polyhedron as a magnetic micro-robot by our folding origami. A tetrahedral magnetic micro-robot was folded to perform a cargo transportation task, which is shown in Fig. 4b. By applying a rotating magnetic field the tetrahedral magnetic robot (Fig. 4b–ii) rotates in the water, generating a liquid flow around the micro-robot carrying surrounding microparticles, which is depicted in Fig. 4b–i. The relationship between velocity of robot and frequency of magnetic field is depicted in Fig. S1 in Supplementary Information. The tetrahedral magnetic robot rotates and locomotes under a rotating magnetic field (10 mT, 5 Hz) with a rotational axis perpendicular to the plane, as shown in Fig. 4b–iii and Supplementary Video 2. The robot rolls along the direction of the rotating magnetic field. During the directional movement the polystyrene microbeads with 5 μm diameter on the bottom surface were driven to move together due to the liquid flow around the tetrahedral magnetic robot. This demonstration shows that our folding origami 3D microstructures can serve as a micro-robot and manipulate micro-objects.

Supplementary video related to this article can be found at https://doi.org/10.1016/j.pnsc.2021.09.010

A twin-jet micro-motor platform with two rolling tubes on both sides and a flat platform in the middle is also demonstrated (Fig. 4c). During the fabrication of this micro-machine, 2 nm Pt was deposited on top of the Ag/Ti/Fe pre-layer. Then, like the fabrication process in Fig. 2a, another multilayer nanomembrane was deposited in the middle of the pre-layer to offset strain gradient of the pre-layer. After being released from the substrate the region in the middle can keep flat while the uncovered regions on both sides roll into microtubes. The Pt layer inside the microtubes can serve as catalyst in hydrogen peroxide solution later. By adjusting the length of the region covered in the middle, twin-jet micromotors with different plane size can be obtained. Two tubular jets on both sides with the Pt catalytic layer on the inner wall can catalyze the decomposition of hydrogen peroxide to generate bubbles to provide a driving force for the motor to move in 5% hydrogen peroxide solution [31] which is shown in Fig. 4c–iii and Supplementary Video 3. The velocity V of the twin-jet micro-motor can be controlled by adjusting the length of the covered region of the middle, which is discussed in detail in Supplementary Note. The flat plane in the middle can potentially be used for the integration of wireless energy transfer coil, light-emitting diodes, and thermo-responsive micro-arm [32], which are all crucial components for multifunctional micro-robots. Moreover, the micro-motor can maintain the flat geometry of the middle plane during locomotion, which ensures the stability of the designed structure. Inspired by the concept of strain design in our folding origami the tubes and flat planes can be obtained in a single micro-structure at the same time. This twin-jet micro-motor platform has wide potentials in micro-robotic applications since functional components can be easily integrated into its flat region.

Supplementary video related to this article can be found at https://doi.org/10.1016/j.pnsc.2021.09.010

4. Conclusion

A new strategy of folding origami is developed based on microdroplet-guided intercalation and strain engineering, which achieves precise geometry control and allows the construction of complex 3D microstructures for micro-machine applications. By sequentially depositing patterned multilayer nanomembranes with designed strain gradients, the strain configuration of local regions can be engineered to create creases (the part where the strain gradient is offset) and facets (the part where the strain gradient remains) for a folding microstructure. The folding angle can be precisely regulated by adjusting the length of crease. Furthermore, a magnetic field can be used to manipulate the folding angle after the folding structure is released.

Potential micro-machine applications among several research areas are demonstrated. The array of micro-folding structure is demonstrated as a magnetic micro-mirror system in optical micro-devices, benefiting from the capability of remote manipulation of facet folding angles using an applied magnetic field. The tetrahedron microstructure is suitable to serve as a functional micro-robot by showing its ability to manipulate micro-objects on a microscopic scale. Besides, inspired by the concept of strain design in our folding origami, a combination of rolling and flat regions is developed to build a twin-jet micro-motor platform, which can be further integrated by electronic circuits and sensor devices to construct more functional micro-machines. The nanomembranes in this concept are not limited to metallic thin films used in this work. Functional 2D materials, such as graphene [33] and magnetic transition metal chalcogenides [34], can also be adapted in this concept to create 3D microstructures with advanced functionalities. These examples indicate the versatility of our origami strategy, which might open a new route for the creating of functional 3D micro-machines.

Declaration of competing interest

The authors declare that they have no known competing financial interests or personal relationships that could have appeared to influence the work reported in this paper.

Acknowledgments

This work is supported by the National Natural Science Foundation of China (Nos. 51961145108, 61975035, and 62005050), the Program of Shanghai Academic Research Leader (No. 19XD1400600), the Shanghai Sailing Program (No. 21YF1401600) and the Science and Technology Innovation Action Plan of Science and Technology Commission of Shanghai Municipality (No. 21ZR1403500, No. 20501130700).

Appendix A. Supplementary data

Supplementary data to this article can be found online at https://doi.org/10.1016/j.pnsc.2021.09.010.

References

[1] J.A. Rogers, Y. Huang, O.G. Schmidt, D.H. Gracias, MRS Bull. 41 (2016) 123–129.
[2] J.A. Rogers, T. Someya, Y. Huang, Science 327 (2010) 1603–1607.
[3] J.A. Rogers, M.G. Lagally, R.G. Nuzzo, Nature 477 (2011) 45–53.
[4] K. Malachowski, M. Jamal, Q. Jin, B. Polat, C.J. Morris, D.H. Gracias, Nano Lett. 14 (2014) 4164–4170.
[5] J.C. Breger, C.K. Yoon, R. Xiao, H.R. Kwag, M.O. Wang, J.P. Fisher, T.D. Nguyen, D.H. Gracias, ACS Appl. Mater. Interfaces 7 (2015) 3398–3405.
[6] T.L. Li, A.N. Zhang, G.B. Shao, M.S. Wei, B. Guo, G.Y. Zhang, L.Q. Li, W. Wang, Adv. Funct. Mater. 28 (2018) 1706066.
[7] F.T. Ji, T.L. Li, S.M. Yu, Z.G. Wu, L. Zhang, ACS Nano 15 (2021) 5118–5128.
[8] T.L. Li, J.X. Li, H.T. Zhang, X.C. Chang, W.P. Song, Y.N. Hu, G.B. Shao, E. Sandraz, G.Y. Zhang, L.Q. Li, J. Wang, Small 12 (2016) 6098–6105.
[9] C. Cui, J. Yin, L. Han, Adv. Funct. Mater. 30 (2020) 2003959.
[10] J.L. Silverberg, A.A. Evans, L. Mcleod, R.C. Hayward, T. Hull, C.D. Santangelo, I. Cohen, Science 345 (2014) 647–650.
[11] J.T.B. Overvelde, T.A. Jong, Y. Shevchenko, S.A. Becerra, G.M. Whitesides, J.C. Weaver, C. Hoberman, K. Bertoldi, Nat. Commun. 7 (2016) 10929.
[12] A.A. Zadpoor, Mater. Horiz. 3 (2016) 371–381.
[13] Z. Liu, A. Cui, J. Li, C. Gu, Adv. Mater. 31 (2019) 1802211.
[14] Y. Zhang, F. Zhang, Z. Yan, Q. Ma, X. Li, Y. Huang, J.A. Rogers, Nat. Rev. Mater. 2 (2017) 17019.
[15] K.E. Laflin, C.J. Morris, T. Muqeem, D.H. Gracias, Appl. Phys. Lett. 101 (2012) 1309.
[16] M. Jamal, A.M. Zarafshar, D.H. Gracias, Nat. Commun. 2 (2011) 527.
[17] D.H. Gracias, Curr. Opin. Chem. Eng. 2 (2013) 112–119.
[18] J. Guan, H. He, D.J. Hansford, L.J. Lee, J. Phys. Chem. B 109 (2005) 23134.
[19] J.H. Cho, T. James, D.H. Gracias, Adv. Mater. 22 (2010) 2320–2324.
[20] R.R.A. Syms, E.M. Yeatman, V.M. Bright, G.M. Whitesides, J Microelectromech Syst 12 (2003) 387–417.
[21] O.G. Schmidt, K. Eberl, Nature 410 (2001) 168.
[22] Y.F. Mei, G.S. Huang, A.A. Solovev, E.B. Ureña, I. Mönch, F. Ding, T. Reindl, R.K.Y. Fu, P.K. Chu, O.G. Schmidt, Adv. Mater. 20 (2008) 3971–4206.
[23] W. Huang, Z. Yang, M.D. Kraman, Q. Wang, Z. Ou, M.M. Rojo, A.S. Yalamarthy, V. Chen, F. Lian, J.H. Ni, Sci. Adv. 6 (2020) 4508.
[24] J.X. Li, J. Zhang, W. Gao, G.S. Huang, Z.F. Di, R. Liu, J. Wang, Y.F. Mei, Adv. Mater. 25 (2013) 3715–3721.

[25] B.R. Xu, X.Y. Zhang, Z.A. Tian, D. Han, X.C. Fan, Y.M. Chen, Z.F. Di, T. Qiu, Y.F. Mei, Nat. Commun. 10 (2019) 5019.
[26] S. Pandey, M. Ewing, A. Kunas, N. Nguyen, D.H. Gracias, G. Menon, Proc. Natl. Acad. Sci. U.S.A. 108 (2011) 19885–19890.
[27] J.H. Na, A.A. Evans, J. Bae, M.C. Chiappelli, C.D. Santangelo, R.J. Lang, T.C. Hull, R.C. Hayward, Adv. Mater. 27 (2015) 79–85.
[28] H.J. In, H. Lee, A.J. Nichol, S.G. Kim, G. Barbastathis, J. Vac. Sci. Technol. 26 (2008) 2509–2512. B.
[29] S. Li, H. Fang, S. Sadeghi, P. Bhovad, K.W. Wang, Adv. Mater. 31 (2019) 1805282.
[30] J.W. Judy, R.S. Muller, J Microelectromech Syst 6 (1997) 249–256.
[31] A.A. Solovev, Y.F. Mei, E.B. Urena, G.S. Huang, O.G. Schmidt, Small 5 (2010) 1688–1692.
[32] V.K. Bandari, N. Yang, D. Karnaushenko, H. Yu, O.G. Schmidt, Nat. Electron. 3 (2020) 172–180.
[33] M.K. Blees, A.W. Barnard, P.A. Rose, S.P. Roberts, K.L. Mcgill, P.Y. Huang, A.R. Ruyack, J.W. Kevek, B. Kobrin, D.A. Muller, Nature 524 (2015) 204–207.
[34] Y.L. Huang, W. Chen, A.T.S. Wee, SmartMat 2 (2021) 139–153.